Journal of Materials Chemistry

Cite this: DOI: 10.1039/c1jm12457a

www.rsc.org/materials

PAPER

New topotactic synthetic route to mesoporous silicon carbide†

Peng-Cheng Gao,[a] Yannick Lei,[a] Andrès F. Cardozo Pérez,[a] Khalil Rajoua,[a] David Zitoun[b] and Frédéric Favier*[a]

Received 31st May 2011, Accepted 5th August 2011
DOI: 10.1039/c1jm12457a

Mesoporous silicon carbide (SiC) was synthesized by a one-pot thermal reduction of SiO_2/C composites by metallic Mg at the remarkably low temperature of 800 °C. Two distinct mesostructured silica were used as hard templates for composite preparation: a hexagonal 3D close-packed assembly of Stöber silica spheres and an ordered mesoporous SBA15 silica. In the latter case, SiC has crystallized in its 2H–SiC hexagonal phase, which is rather unique at such a low temperature. Composites were obtained by impregnation/polymerisation/carbonisation of a molecular carbon precursor within the porous structure of the silica template. After thermal treatment at a moderate temperature in the presence of Mg and subsequent by-products rinsing off, both prepared SiC showed distinct mesoporous structures related to the initial SiO_2 architectures. By comparison of the mesoporous characteristics, resulting SiC was found to retain the carbon structures of the pristine composites. The description of the synthetic mechanism of this topotactic reaction contrasts with the usual assumption stating the templating role of silica.

Introduction

Chemical, mechanical, and thermal stabilities are tremendous characteristics of metal carbides. Thanks to these characteristics and their remarkable thermal conductivity, they fit a broad spectrum of applications in harsh or hostile environments such as diesel particulate filters,[1] spacecraft coating,[2] structural material for fusion reactors,[3] and substrate material for high-temperature gas sensors.[4] For example, silicon carbide (SiC) competes with diamond as a low cost hard material (9.5 on the Mohs scale).[5] SiC is also a well known semiconducting material having a good electrical conductivity and displaying a band gap between 2.2 and 3.3 eV,[4] depending on the polytype considered (3C, 4H, 6H–SiC, according to the crystal lattice, C for cubic or H for hexagonal). Thus, it shows matching characteristics for high-temperature, high-power and/or high-frequency microelectronics devices. However, optical applications remain limited because of low light quantum yield originating from an indirect band gap.[6] Going to the nanoscale should enhance its optical properties,[7] as well as its potential technological applications in the fields of surface chemistry and physics.

Several synthetic routes have recently been investigated for nano or mesostructured SiC material. Except from the routes using Si wafers and CVD-assisted deposition[8] or epitaxial growth,[9] synthesis of nano-SiC has been performed using either high pressure and/or high temperature processes. Right after the first attempt by Zhou *et al.* from reacting carbon nanotubes with SiO vapor,[10] carbide nanorods or bamboo-like SiC were obtained by carbothermal reactions.[11,12] Polycarbosilanes were also considered as suitable chemical precursors as they are a unique source of both Si and C for the pyrolytic preparation at 1400 °C of SiC fibers (3C–SiC) by the Yajima synthetic route.[13,14] Wang and Li used alumina membranes as a mesoporous template for the fabrication of SiC tubular arrays by polycarbosilanes pyrolysis at 1250 °C.[15] More recently, Zou *et al.* synthesized 2H–SiC nanoflakes by autoclaving CaC_2 and $SiCl_4$ at 180 °C for 36 h. This reaction at moderate temperature originates from "the high energy" contained in CaC_2.[16] Using another route, Zhao Zhang *et al.* prepared 3C–SiC nanorods at high temperature (1700 °C) through the decomposition of a polysilazane precursor to a-SiCN at 1000 °C.[17] In a more recent report, Gedanken *et al.* presented nanostructured SiC obtained by reaction under autogenic pressure at an elevated temperature (RAPET) through thermolysis of triethylsilane or cheaper silicone oil.[18]

The chemical stability of SiC, as well as of some other metal carbides,[19] could be advantageous for the replacement of conventional catalyst supports in heterogeneous catalysis.[20] It does not react with the active phase and allows catalyst regeneration in extreme oxidative/reductive conditions without structural damage while quickly accommodating large temperature gradients and mechanical constraints. Moreover, Claridge *et al.*

[a]*Institut Charles Gerhardt Montpellier UMR 5253 CNRS, Université Montpellier 2, cc1502, 34095 Montpellier cedex 05, France. E-mail: fredf@um2.fr; Fax: +33 (0)4 67 14 33 04; Tel: +33 (04) 67 14 33 32*
[b]*Bar Ilan University, Department of Chemistry and Institute of Nanotechnology and Advanced Materials, Ramat Gan, Israel. E-mail: david.zitoun@biu.ac.il; Fax: +972 (0)3 738 40 53; Tel: +972 (0)3 738 45 12*

† Electronic supplementary information (ESI) available: Raman spectra of prepared SiC materials, XRD patterns of reaction products from SiO_2 and carbon black mixture, and corresponding Raman spectrum. See DOI: 10.1039/c1jm12457a

demonstrated that the use of SiC could prevent the carbon poisoning of the supported catalyst surface.[21] For such applications as well as for the fabrication of bio-implants[22] for instance, an increase in the surface developed by the carbide material is a critical parameter and remains the main motivation for the development of original methods for the preparation of mesoporous SiC.

The route to porous SiC generally proceeds by using various porous siliceous templates for the impregnation of a carbonaceous precursor at the pore surface and within the porous volume. The main challenge lies in maintaining the template structure during the SiC synthesis. This synthetic approach leads to various mesoporous SiC showing defined structures and morphologies. Mesoporous silica or silica porogens are usually used as templates impregnated with molecular carbonaceous precursors in vapor, liquid (*i.e.* monomers) or polymerized form. After carbothermal reduction at high temperature, by-products, usually unreacted C and silica, are removed by oxidation and HF dissolution, respectively.[20–28]

Because of synthesis temperatures generally being above 1200 °C, material sintering cannot be prevented thus leading to limited surface areas and extended material aggregation.[28] Among the reported synthetic routes, the use of a reductive reagent such as H_2 introduced by Krawiec *et al.* allows a drastic decrease of the thermal treatment temperature, down to about 900 °C.[26] Correlatively, the recent and successful reduction of the nanostructured silica of diatoms (frustules) to silicon replica using Mg at 650 °C performed by Bao *et al.* appeared to us as an attractive opportunity on the route to nanostructured SiC.[29] This approach was confirmed by Gedanken *et al.* for the preparation of high surface area Si from Stöber silica and Mediterranean sand.[30] By the time the present study was developed, Hu and Stucky succeeded in the synthesis of a macro/mesoporous SiC at temperatures ranging from 600 to 800 °C.[31] Although they demonstrated the use of Mg as an efficient reducing agent for SiC preparation through a pseudomorphic transformation at moderate temperature, their synthetic route imposes the preliminary synthesis of a hierarchically ordered porous SiO_2/C nanocomposite.

In the present paper, we report on a simpler synthesis of porous SiC by performing a topotactic thermal reduction by magnesium of a composite material made of a carbon framework templated by silica porogens. Therefore, the reduction of SiO_2/C composites to SiC is achievable at relatively low temperature (below 800 °C). Moreover the carbon framework and structure, as a replica of the pristine silica template, either mesoporous or porogen assembly, are retained by the final SiC product. The crystal structure of the mesoporous SiC has been found to highly depend on the porosity of the carbon replica, resulting in a cubic structure 3C–SiC in the case of macro-porogens and hexagonal structure 2H–SiC in the case of meso-porogens.

Experimental section

1 Synthesis of the composite precursors SiO_2/C

The first composite precursor referenced thereafter as SiO_2-Stöber/C was prepared according to a previously reported method.[32] It was synthesized from silica spheres that were prepared following the Stöber method.[33] Briefly, 24 g of tetraethoxysilane (TEOS, 98%, ACROS Organics) were added to 720 mL of anhydrous ethanol (EtOH, denatured with 5% MEK, ACROS Organics) and 4 g of water. Then, 48 g of ammonia (NH_4OH, 28%, VWR) were added. The spheres were collected by evaporation under vacuum. 3D-assemblies were obtained by slow evaporation of suspended spheres. A thermal treatment at 800 °C for 4 hours was performed to enhance the contact between the spheres. Then the assemblies were impregnated by furfuryl alcohol, which was polymerised at 80 °C in air and carbonised at 800 °C under N_2 flow for 16 h. The second precursor (SiO_2-SBA15/C) was obtained with a SBA15 2D-hexagonal mesoporous silica as the silica template.[34] It was prepared following the synthetic route described by Szczodrowski *et al.*[35] using triethoxysilane (TEOS) as silica precursor and a Pluronic triblock copolymer (P_{123}) as templating agent: TEOS/P_{123}/HCl/H_2O (molar ratios 1.0 : 0.017 : 5.7 : 191.8). Briefly, P_{123} (Aldrich) was dissolved in water overnight and then HCl was added for 1 h before the addition of TEOS. The obtained solution was put in an autoclave at 100 °C for 24 h. P_{123} soft template was removed by calcination at 540 °C. Then the composite SiO_2-SBA15/C was obtained by the carbonisation of furfuryl alcohol (FA, 98% GC, Aldrich) in the same way as for SiO_2-Stöber/C.

2 Magnesio-thermal treatment of the precursors

Following a similar process to reduce silica to silicon as described by Bao *et al.*,[29] composite precursors (SiO_2-Stöber/C and SiO_2-SBA15/C) were both thermally treated in the presence of metallic Mg powder. As a general approach for the synthesis of metal carbide, this procedure is known as magnesiothermic reduction.[36,37] In a few words, in a glove box filled with Ar, the precursor was manually mixed with a 10% molar excess of metallic Mg in a stainless steel 316L tube sealed under Ar. The magnesio-thermal treatment was performed at 800 °C for 24 h with a heating rate of 2 °C min^{-1}.

3 Purification of the synthesised powders

To eliminate reaction by-products, including MgO and Mg_2Si, the synthesized powders were rinsed by slowly adding H_2SO_4 (95–97%, Fluka). Thereafter a mixture of EtOH/HF/H_2O (0.8 : 0.1 : 0.1) (HF, 40%, VWR) was used until the complete dissolution of unreacted Si as confirmed by XRD (Fig. 1) and EDX analysis (Table 1). A thermal treatment was performed at 800 °C for 12 h to eliminate unreacted carbon. The product colour faded from dark brown to pale yellow. Final products were identified as pure SiC and will be referenced in the following as SiC-Stöber and SiC-SBA15 depending on their respective SiO_2/C precursor.

4 Characterisations of the powder

X-Ray diffraction (XRD) patterns were measured at the various purification steps using a Phillips X'Pert diffractometer (CuKα1) in Bragg–Brentano configuration. Samples were also imaged by scanning and transmission electron microscopies using a JEOL JSM-6300F scanning electron microscope (SEM) and a JEOL 1200 EX2 TEM microscope operating at 100 kV. Energy

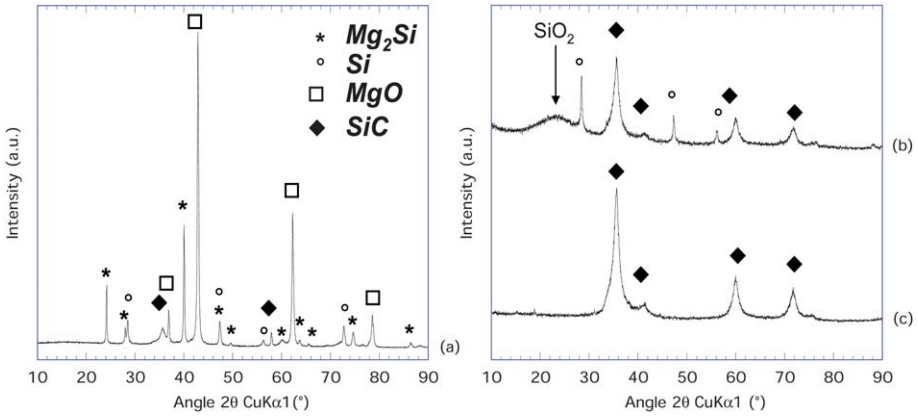

Fig. 1 XRD patterns of SiC-Stöber material as synthesized (a), after H_2SO_4 treatment (b) and after EtOH/HF/H_2O treatment and thermolysis in air (c).

Dispersive X-ray analyses (EDX) were done using FEI Quanta 200 equipment on powders dispersed on a nickel foil. Surface areas were calculated by the Brunauer–Emmett–Teller (BET) method from adsorption isotherms of N_2 obtained at 77.4 K. The experimental adsorption isotherms were measured using Micromeritics ASAP equipment. Porous characteristics were extracted using the αs plot method.[38] Raman spectra were recorded using a Labram ARAMIS IR spectrometer from Horiba-Jobin Yvon operated using a He/Ne laser ($\lambda = 633$ nm).

Results

1 Synthesis and characterisations of SiC-Stöber

XRD patterns were recorded at various steps of the purification process for the SiC-Stöber (Fig. 1). Fig. 1a was obtained for the as-synthesized powder from magnesio-thermal reaction in the stainless steel tube and without any post-treatment. It is actually composed of four different phases, which are a cubic form of silicon carbide (◆ 3C–SiC, JCPDS#29-1129), silicon (○ Si, JCPDS#27-1402), magnesium oxide (□ MgO, JCPDS#45-0946) and Mg_2Si (*, JCPDS#35-0773). Fig. 1b depicts the XRD pattern measured after H_2SO_4 treatment. It shows that the Mg-containing phases have been thoroughly eliminated whereas SiC (◆) was not affected by this acidic treatment. Most of Si (○) remains, however, part of it was oxidised into silica by the direct effect of H_2SO_4. The pattern obtained after the treatment with a mixture of EtOH/HF/H_2O shows that only 3C–SiC (◆) remains at this purification step. Although carbon XRD features were not observed, the black color of this powder suggests the presence of carbon traces. After a thermal treatment under air was performed, the final color of the recovered SiC-Stöber powder was grayish without any changes in the XRD features of the resulting powder (Fig. 1c).

Table 1 Energy dispersive X-ray analysis of prepared SiC-SBA15 and SiC-Stöber. All results are in atomic %

Element composition	C	O	F	Mg	Si
SiC-SBA15	46 ± 3	4.6 ± 0.	3.3 ± 0.2	3.0 ± 0.2	43 ± 3
SiC-Stöber	45 ± 3	8.0 ± 0.4	1.1 ± 0.1	1.1 ± 0.1	45 ± 3

SEM micrographs of SiC-Stöber (Fig. 2b) show that the porous structure is built on spherical pores of about 150 nm in diameter in the present case. The pore size, shape and organisation correspond to those of the initial template made of a 3D-assembly of silica spheres. This negative replica structure is very close to that of the mesoporous carbon (C-Stöber, Fig. 2a) obtained after dissolution of the silica sphere assembly template as previously prepared.[33] In comparison, the regular honey-comb structure obtained for the previously prepared C-Stöber (Fig. 2a) seemed more difficult to achieve with SiC-Stöber. If part of the hexagonal honeycomb ordering is lost, most of the shape features are however retained.

TEM pictures confirm that template characteristics are retained in the resulting SiC-Stöber material (Fig. 3b). Walls appear as composed of aggregated grains of SiC. In contrast, carbon walls in C-Stöber look denser (Fig. 3a). It is noteworthy that the electron diffraction performed on the synthesized powder confirmed the cubic 3C–SiC crystallographic phase (Fig. 3c). Although EDX analysis (Table 1) shows the presence of O, Mg and F traces, it also indicates a Si/C atomic ratio close to 1 (0.94) confirming the preparation of stoichiometric SiC material. Measured oxygen comes mostly from residual absorbed di-oxygen from air. The calculation of the surface area by the BET method from the adsorption isotherm of N_2 performed at 77.4 K on SiC-Stöber gives values up to 90 $m^2\ g^{-1}$ (Table 2). SiC-Stöber retains only $1/10^{th}$ of the large surface area at 900 $m^2\ g^{-1}$ developed by C-Stöber through the meso/microporous structure of the carbon walls. During conversion from pristine carbon to SiC, most of this porosity is lost as demonstrated by the large surface area decrease. These values have however to be compared to the geometrical area calculated at 9.2 $m^2\ g^{-1}$ for ideal mesoporous

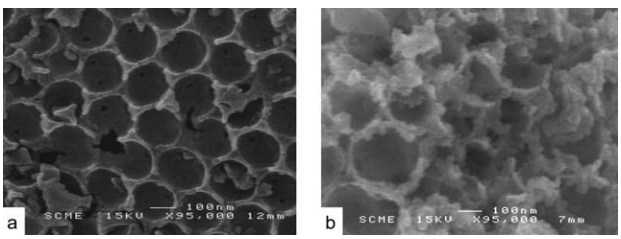

Fig. 2 SEM pictures of the mesoporous carbon (a) and the porous SiC (b).

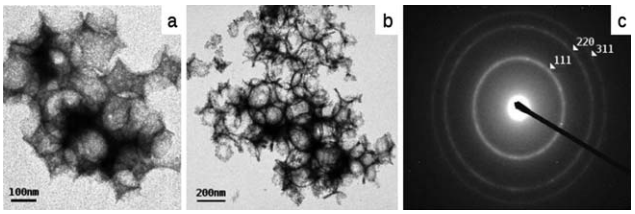

Fig. 3 TEM pictures of mesoporous carbon (a), porous SiC (b) and electron diffraction on SiC (c).

SiC built on a regular hexagonal 3D-arragement of spherical pores of 150 nm in diameter. This discrepancy lies in the meso/microporosity developed by the granular walls of SiC-Stöber as observed by TEM.

The Raman spectrum measured from 150–1200 cm^{-1} on SiC-Stöber (Fig. S1, ESI†) shows a series of 4 broad bands characteristic of SiC material.[39,40] Low wavelength number peaks correspond to high energy network vibration modes at 195 and 412 cm^{-1}. The peaks in the 600–1000 cm^{-1} range correspond to longitudinal (LO) and transverse (TO) optical peaks respectively at 865 and 762 cm^{-1}. As confirmed by LO and TO relative intensities, no anisotropy is observed for the prepared SiC-Stöber.

2 Synthesis and characterisation of SiC-SBA15

To demonstrate the versatility of the presented synthetic route to porous SiC, another silica source was used as the precursor, namely a laboratory prepared mesoporous SBA15 silica.[35] The synthetic SiO_2-SBA15 was used as prepared.

XRD measurements show that the powder synthesized from heating SiO_2-SBA15/C in the presence of Mg at 800 °C (Fig. 4a) is a mixture of four phases: SiC (◆), Si (○), MgO (□) and Mg_2Si (*). The sulfuric acid treatment confirmed its efficiency in rinsing-off all the Mg-containing phases. Peaks characteristic of MgO and Mg_2Si by-products obviously disappeared while those from 3C–SiC remained. However some narrow and weak peaks were also observed in the $10° < 2\theta < 30°$ range (Fig. 4b) demonstrating the presence of unidentified impurities trapped in the mesoporous structure of the SBA15-like material.

Nonetheless, the HF/EtOH treatment allowed elimination of most of those impurities (Fig. 4c). The remaining peaks may be attributed to silica, proving that the treatment was not fully effective even after 2 days of contact. The broad peak centered at $2\theta = 36°$ characteristic of a poorly crystallized 3C–SiC appeared

Table 2 Specific surface areas calculated by the BET method for the various mesoporous materials prepared in this work. Pore volume and size are extracted from BET analysis. The wall size are measured from TEM/SEM micrographs

Sample	S_{BET}/ $m^2\ g^{-1}$	Pore volume/ $cm^3\ g^{-1}$	Pore size/ nm	Wall size/ nm
SiO_2-Stöber	23 ± 2	0.25	40.5	n.a.
C-Stöber	900 ± 30	0.39	2.8	21
C/SiO_2-Stöber	474 ± 10	0.09	20.4	—
SiC-Stöber	90 ± 1	0.27	21.4	30
SiO_2-SBA15	760 ± 10	0.65	4.7	5.2
C-SBA15	1130 ± 4	0.81	3.1	4.0
C/SiO_2-SBA15	425 ± 4	0.43	4.0	—
SiC-SBA15	450 ± 1	0.48	4.4	7.2

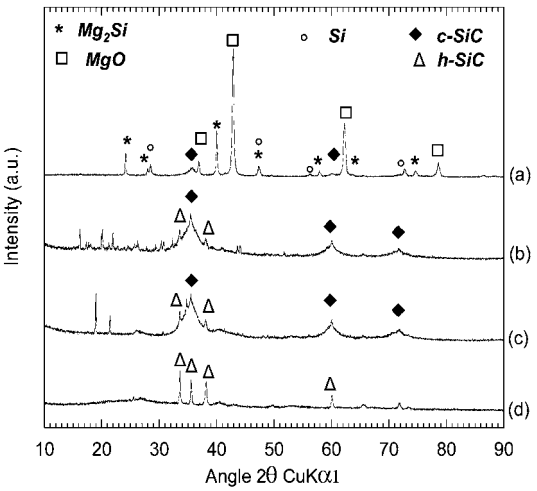

Fig. 4 XRD patterns of SiC-SBA15 as-synthesised (a), after H_2SO_4 treatment (b), after HF/EtOH treatment (c), and after thermal treatment (d).

to show a complex structure with small peaks corresponding to the hexagonal-latticed SiC. The sample then underwent a thermal treatment at 800 °C for 12 h in order to remove traces of the remaining carbon, resulting in the complete phase transition from 3C–SiC like cubic phase into 2H–SiC hexagonal structure (Fig. 4d, JCPDS# 73-1749).

Although EDX analysis (Table 1) shows the presence of O, Mg and F impurities, it also indicates a Si/C atomic ratio equal to 1 (~1.002) confirming the preparation of stoichiometric SiC material.

TEM pictures depicted in Fig. 5 allow the comparison of the mesostructure of resulting SiC with that of the starting SBA15 silica. Vermicular mesopores can be unambiguously observed in the SiC-SBA15 structures (Fig. 5b and inset). The characteristic hexagonal pore ordering of SiO_2-SBA15 (Fig. 5a) is obviously lost during the carbide conversion because of a defective replication.

These changes in the porous structure are confirmed by comparative XRD measurements at small angles depicted in Fig. 6. The diffraction peak at 0.805 °2θ corresponds to the SBA15 inter-pore distance at 5.5 nm. For the corresponding C-SBA15, this peak is slightly shifted at 0.825 °2θ (5.3 nm) as a broad shoulder in the absorption peak. The decrease of the peak intensity, when compared to that of SiO_2-SBA15, is characteristic of a partial loss in the pore ordering from defective templating of SiO_2 to the corresponding C. This loss is even enhanced for SiC-SBA15 for which the corresponding diffraction peak disappears since very low shoulders in the absorption peak cannot be reasonably assigned.

As for SiC-Stöber, Raman peaks in the 600–1000 cm^{-1} range are characteristics of the isotropic SiC material with LO and TO peaks at 873 and 765 cm^{-1} respectively (Fig. S1, ESI†).

BET measurements confirm the mesoporous characteristics of both prepared SiO_2-SBA15 and SiC-SBA15 replica showing up to 760 $m^2\ g^{-1}$ and 450 $m^2\ g^{-1}$ surface areas, respectively (Table 2). This surface area decrease is characteristic of a partial loss of the mesoporous volume during carbide conversion.

Discussion

From these first experimental results on the magnesio-thermal reduction of SiO_2/C composites towards nanostructured SiC, the main discussion lies in the elucidation of the synthetic mechanism from the silica template to the resulting SiC replica, especially on the critical parameters that impact the chemical nature and morphological characteristics of the resulting material.

For both Stöber- and SBA-based materials, SiO_2/C composites are obtained by *in situ* carbonisation in the dense SiO_2/polyfurfuryl composites of polyfurfuryl within the silica mesostructure. This carbonisation results in the shrinkage of the carbonaceous precursor leading to a (re-)opening of the porous volume in resulting SiO_2/C composites. This open structure allows Mg in the melt to enter the mesopores for the efficient reduction of SiO_2, as proven by MgO by-product, and subsequent conversion of the SiO_2/C composite into SiC.

As shown by EDX, SiC showing silicon/carbon ratios close to 1 have been obtained from SiO_2/polyfurfuryl composites demonstrating furfuryl alcohol as suited carbon precursor for such a synthetic approach. In the conventional carbo-reduction route, carbon precursors with higher carbon yield such as sucrose or carbon obtained by gas phase cracking using acetylene or propylene are usually preferred since a large excess of carbon is needed in the SiO_2/C composite: schematically, part of it is used for the reduction of SiO_2 to gaseous SiO while the rest of it should be available to react with generated SiO to form SiC. In the present work, the reaction temperature limited to 800 °C is not high enough to allow any carbo-reduction. At the chosen temperature, any carbon is consumed for SiO_2 reduction since melting Mg is the actual silica reducing agent. The whole carbon in the composite is then available for reaction with silicon for SiC generation. Despite a low carbon yield from furfuryl alcohol, the carbon content in the composite is obviously sufficient for the preparation of stoichiometric SiC.

Mg_2Si side-product formation was evidenced by XRD during SiC syntheses and easily removed by H_2SO_4 treatment. In contrast, the formation of MgC_2, which could have been considered for obvious reasons, is kinetically disfavored in the presence of any oxygen source and does not compete with MgO which is preferentially generated.[41]

Composite material *versus* mixture

For both SiC-Stöber and SiC-SBA15 materials, precursors are SiO_2/C composites as simultaneous sources of Si and C. Is it absolutely necessary to use such composite precursors or would it be possible to prepare SiC starting from a simple mixture of SiO_2 and carbon?

To address this question, 3D-assemblies of SiO_2-Stöber spheres were manually ground together with acetylene black carbon at the same weight ratio as for the SiO_2-Stöber/C precursor material, *i.e.* 10 wt% SiO_2 in carbon as determined by TGA experiment (data not shown). The thermal reduction by Mg was then processed as described above for SiO_2/C composites (same sampling, thermal treatment at 800 °C for 12 h). The synthesised powder was characterised by XRD measurements through the purification process (Fig. S2, ESI†) and the results demonstrated the simultaneous presence of Mg_2Si, MgO and Si without any trace of SiC in any expected crystallographic 3C or 2H forms (no fingerprint at $2\theta = 35°$). In contrast, both XRD pattern and Raman spectrum (Fig. S3, ESI†) of the material at the final purification step showed the presence of Si (obviously together with amorphous C). Acetylene black and SiO_2-Stöber are very finely dispersed powders that were intimately mixed but despite our efforts it was not possible to prepare SiC from this mixture. At the operating temperature, carbon does not react and only Si can be obtained by direct reduction of SiO_2 by Mg. It can then be stated that the conversion from SiO_2/C to SiC is preferentially achieved at the SiO_2/C interface when SiO_2 and C are used as composite precursors rather than as a simple mixture.

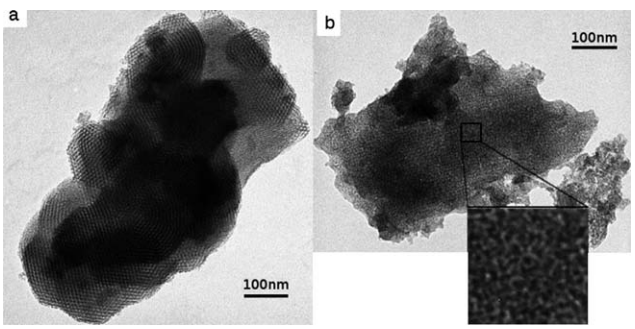

Fig. 5 TEM pictures of SBA15 silica material (a) and SiC-SBA15 (b).

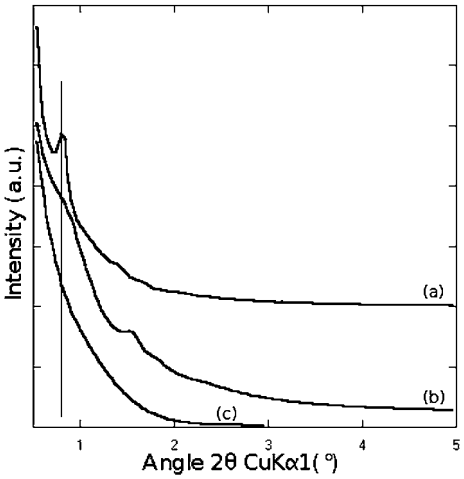

Fig. 6 XRD patterns at small angles for SBA15 silica material (a), C-SBA15 (b), SiC-SBA15 (c).

Templating effect

Mesoporous SiC has been previously prepared through high temperature carbo-reduction processes using silica as the hard template impregnated with a carbon precursor. In contrast with usual template reactions for which the template should be removed to open the porosity, for SiC syntheses, the template is chemically converted during the reaction while keeping its initial shape and morphology. SiO_2 is usually stated as the material template without any anticipation on the reaction mechanism. Alternatively, in the Hu and Stucky approach, the precursor is first prepared as a macro/mesoporous SiO_2/C composite which is

converted by magnesiothermic reduction though a pseudomorphic mechanism retaining the ordered porous structure of the composite material.[31]

However, in a mesoporous silica/carbon precursor such as SBA15/sucrose for example, both replica and inverse replica look similar in many ways, *i.e.* carbon and silica are replicas showing the same structure and morphology.[42] During the conversion, one among them "dissolves" to give SiC showing the same structure as the initial template. The question however remains as to which, from SiO_2 or C, actually plays the role of the template.

The topotactic reaction to this covalent carbide implies the reduction of Si^{4+} to Si(0) by Mg through the chemical pathway depicted in Scheme 1.

$$SiO_2/C + 2Mg \rightarrow SiC + 2MgO$$

Scheme 1 Reaction pathway for the magnesiothermal reduction of SiO_2/C composite as SiC.

SiC is then formed by solid state reaction of reduced Si with C at the reaction temperature. Considering the templating effect, this reaction obviously implies the diffusion of one of these elements into the other structure. Without any anticipation of the diffusion properties of both Si and C at the reaction temperature, it is *a priori* difficult to conclude if C diffuses into the Si structure or the other way around with a diffusion of Si into the C framework.

In our study, the use of two distinct silica templates helped us to refine the microscopic conversion mechanism. Using SBA15/C composite, the resulting SiC shows a disordered porous structure close to that of SBA15 or its indistinguishable carbon replica. On the other hand, the SiO_2-Stöber/C composite is obtained from SiO_2 spheres building a hexagonal packed assembly with voids in between spheres filled-up with a carbon precursor. After carbonisation under neutral atmosphere, the silica template can be removed from the SiO_2/C composite to open the porosity and the resulting mesoporous C-Stöber shows a spherical honeycomb-like porous structure (Fig. 2a) as inverse replica of the sphere assembly. The resulting SiC-Stöber structure (Fig. 2b) is very close to that of C-Stöber suggesting that the carbon structure acts as actual template rather than the silica sphere assembly. Reaction proceeds by simultaneous reduction of silica and solid-state diffusion of silicon into the carbon walls to give the corresponding SiC. In the case of SiC-Stöber, the microporosity developed into the rather thick carbon walls is highly favourable to the Si diffusion process. In SBA15 derived material, carbon walls are very thin and diffusion proceeds easily through the entire carbon framework. For both Stöber and SBA15 based materials, the increases of the measured wall thicknesses (Table 2) from C to SiC are lower than expected by considering the corresponding material molar volumes at 5.3 $cm^3\ mol^{-1}$ and 12.5 $cm^3\ mol^{-1}$ for C and SiC respectively. This is characteristic of a low density highly defective or (micro)porous carbon.

The granular structure of SiC-Stöber, as demonstrated by TEM, could be explained by a limited conversion of carbon into SiC originating from a lack of silica available in the composite structure for a complete conversion. After burning in air the remaining carbon, grain boundaries and intergrain cracks appeared. A limited solid state diffusion of Si at the reaction temperature or specific nucleation-growth processes of SiC at 800 °C could also account for this granular wall morphology.

These changes in the morphologies at the nanoscale, as demonstrated by the loss of microporosity in Stöber derived material or the loss of mesoporous hexagonal ordering in SiC-SBA15, account for the mechanical stress encountered by the material during the chemical conversion from SiO_2/C composites to the resulting SiC. This topotactic reaction proceeds by chemical reduction of SiO_2 in Si ad-atoms that diffuse through the carbon framework resulting in the SiC formation. From the crystallographic point of view, this reaction consists of a conversion from amorphous C with hexagonal short range ordering to cubic like SiC. Cubic SiC shows a diamond structure very close to that of a C diamond ($F\bar{4}3m$) in which 4C atoms in tetrahedral sites are replaced by Si atoms. Such conversion from hexagonal (or disordered) carbon to a diamond structure has already been extensively studied including a detailed structural identification and description of intermediates.[43] At the atomic scale, Si atoms progressively diffuse in between the carbon graphene layers. Formed Si–C interactions (bonds) disrupt the C6 π system until C–C bonds break and Si replace C atoms to give a Si/C atomic stoichiometry of 1. At some point, the energy provided to the system allows an atomic rearrangement to give a diamond 3C–SiC structure.

Indeed, 3C–SiC is obtained from SiO_2-Stöber/C after thermal carbon purification at 800 °C under air, whereas, following the same process, 2H–SiC is obtained from the SBA15/C composite precursor. The fact that two crystallographically distinct SiC forms are obtained depending on the precursor mesostructure suggests that 3C–SiC and 2H–SiC have a kinetically controlled growth mechanism. The diffusion of Si atoms is assumed to be the driving force of the reaction. The magnesium has to enter the porous structure to react with silica in a liquid or gaseous form. Taking into account the very small pore radius of the SBA15/C mesostructure (3.1 nm), only gaseous diffusion should occur resulting in a SiC growth rate slower than in the case of Mg liquid diffusion. Moreover the smaller pores promote higher adsorption potential of gaseous Mg at the pore surface that slow down the SiC growth rate. Therefore, the formation of the high temperature thermodynamically stable phase 2H–SiC is thought to result from the lower growth rate compared to the low temperature 3C–SiC observed using SiO_2-Stöber/C precursor. In the latter case, the liquid diffusion of Mg into the macroporous structure of SiO_2-Stöber/C favours the formation of the low temperature 3C–SiC phase. The porosity of the initial structure directs not only the SiC morphology but also its crystal structure. The formation of the high temperature 2H–SiC through such a low temperature process is remarkable and has not been reported so far when using a templating synthesis pathway.

The SiC-Stöber material showed a significant loss of the surface area when compared to the porous C-Stöber. Indeed, the SiC material exhibits a surface area up to 90 $m^2\ g^{-1}$, while the surface area measured for the mesoporous carbon reached up to 900 $m^2\ g^{-1}$.[33] This loss cannot be attributed only to the material density increase from C to SiC (from 2.27 to 3.22). Actually, the large surface area of C-Stöber has been shown to mostly originate from the microporosity in the carbon walls while the

geometrical area is rather limited to about 9 $m^2 g^{-1}$ (for C-Stöber prepared from 150 nm in diameter silica spheres). In the present case, this loss of one order of magnitude in the measured specific areas from mesoporous carbon to mesoporous SiC points out the loss of microporosity of the carbon walls, which may be due to the micropore collapsing during SiC formation. Some microporosity however remains thanks to the granular morphology of the walls in SiC-Stöber. This trend is corroborated by the changes in pore volumes from C-Stöber to SiC-Stöber (Table 2). In contrast, the carbon honeycomb mesostructure is not affected by this reaction since it is retained by the resulting SiC.

As for SiC-Stöber, there are drastic decreases in both surface area and pore volume through the conversion from C-SBA15 (or SBA15) to SiC-SBA15. Contributions in surface area and pore volume changes between SBA15 silica and SBA15-SiC due to change in material densities can be determined by using the following formulae:

$$S_{SiO_2} = S_{SiC}\frac{d_{SiO_2}}{d_{SiC}} \text{ and}$$

$$V_{pore,SiO_2} = V_{pore,SiC}\frac{d_{SiO_2}}{d_{SiC}} \text{ with } d_{SiO_2} = 2.32 \text{ and } d_{SiC} = 3.22$$

Then S_{SiC} and $V_{pore,SiC}$ are calculated at about 550 $m^2 g^{-1}$ and 0.47 $cm^3 g^{-1}$, respectively. These values are slightly larger than those measured for SiC-SBA15 at 450 $m^2 g^{-1}$ and 0.48 $cm^3 g^{-1}$ (Table 2). These losses in the surface area and pore volume cannot be explained only by the intrinsic change in the density of the material that occurred during the conversion from SiO_2 to SiC.

When considering carbon ($d_C = 2.27$) as template, decreases in porous characteristics cannot either be explained only by a simple change of density. Indeed, calculated S_{SiC} and $V_{pore,SiC}$ at about 800 $m^2 g^{-1}$ and 0.57 $cm^3 g^{-1}$, respectively, are found to be greater than the measured ones at 450 $m^2 g^{-1}$ and 0.48 $cm^3 g^{-1}$, respectively.

These changes are characteristic of the profound modifications of the porous structure encountered by SiC-SBA15 precursors through the high mechanical stress occurring during the chemical conversion. Changes are not only limited by a loss in the porous ordering as demonstrated by TEM imaging but also by a partial collapsing of the porous volume.

Comparison with data from SiC-Stöber material and precursors suggests that the mechanical stress impact of the chemical conversion is lower on mesoporous material rather than on microporous compounds. The surface area decrease is limited to less than a third from C-SBA15 to SiC-SBA15, while only 10% of the initial surface area developed by C-Stöber is retained in the final SiC-Stöber (Table 2).

Conclusions

Mesoporous SiC was synthesized in a one-pot thermal reduction of SiO_2/C composites by metallic Mg at the very low temperature of 800 °C. XRD patterns, electron diffraction and Raman spectroscopy confirmed that, after purification, pure SiC was obtained. SEM and TEM pictures showed that the porous structure of the carbon was conserved in the final SiC material. The crystallographic phase obtained depends on the precursor used, 3C–SiC and 2H–SiC, for Stober-SiC and SiC-SBA15 respectively. The formation of the high temperature 2H–SiC through such a low temperature process is remarkable and has not been reported so far when using a templating synthesis pathway. Furthermore, the ability to design a porous silicon carbide with different polytypes could be used to tune the electronic properties of the porous material. The comparison between the precursor and the product morphology points out that the specific synthetic mechanism in such topotactic reactions proceeds by solid state diffusion of Si into the carbon structure at the reaction temperature. This very versatile method has been shown to lead successfully to materials with a porosity as high as 450 $m^2 g^{-1}$.

Acknowledgements

CNRS is gratefully acknowledged for the funding, Y.L. thanks the French ministry of Research and Education and P-C.G. the China Scholarship Council for PhD fellowships. The Technical staff of Institute Charles Gerhardt Montpellier and especially David Bourgogne are fully acknowledged for Raman microspectroscopy measurements. Professor Aharon Gedanken is deeply thanked for the motivating discussion.

Notes and references

1 D. Fino, *Sci. Technol. Adv. Mater.*, 2007, **8**, 93.
2 K. Kato, *Materialwiss. Werkstofftech.*, 2003, **34**, 1003.
3 S. J. Zinkle and N. M. Ghoniem, *Fusion Eng. Des.*, 2000, **51**(2), 55.
4 N. G. Wright, A. B. Horsfall and K. Vassilevski, *Mater. Today*, 2008, **11**, 16.
5 H. F. Mark, D. F. Othmer, C. G. Overberger and G. T. Seaborg, in *Kirk-Othmer Encyclopedia of Chemical Technology*, John Wiley & Sons, New York, 3rd edn, 1978, vol. 4.
6 L. Hoffmann, G. Ziegler, D. Theis and C. Weyrich, *J. Appl. Phys.*, 1982, **53**, 6962.
7 J. Y. Fan, X. L. Wu and P. K. Chu, *Prog. Mater. Sci.*, 2006, **51**, 983.
8 G. Shen, Y. Bando, C. Ye, B. Liu and D. Golberg, *Nanotechnology*, 2006, 3468.
9 L. T. Canham, *Appl. Phys. Lett.*, 1980, **57**, 1046.
10 D. Zhou and S. Seraphin, *Chem. Phys. Lett.*, 1994, **222**, 233.
11 H. Dai, E. W. Wong, Y. Z. Lu, S. Fan and C. M. Lieber, *Nature*, 1995, **375**, 769.
12 Y.-J. Hao, G.-Q. Jin, X.-D. Han and X.-Y. Guo, *Mater. Lett.*, 2006, **60**, 1334.
13 J. Y. Fan, X. L. Wu and P. Chu, *Prog. Mater. Sci.*, 2006, **51**, 983.
14 Y. Meng, D. H. Chen, S. J. Cheng, P. Chen, T. F. Yang, Y. Wan and D. Y. Zhao, *Adv. Funct. Mater.*, 2006, **16**, 561.
15 H. Wang, X. D. Li, T. S. Kim and D. P. Kim, *Appl. Phys. Lett.*, 2005, **86**, 173104.
16 G. F. Zou, C. Dong, K. Xiong, H. Li, C. L. Jiang and Y. T. Qian, *Appl. Phys. Lett.*, 2006, **88**, 071913.
17 L. G. Zhang, W. Y. Yang, H. Jin, Z. H. Zheng, Z. P. Xie, H. Z. Miao and L. N. An, *Appl. Phys. Lett.*, 2006, **89**, 143101.
18 V. G. Pol, S. V. Pol and A. Gedanken, *Eur. J. Inorg. Chem.*, 2009, 709.
19 N. I. Ilchenko, Y. I. Pyatnitsky and N. V. Pavlenko, *Teoreticheskaya I Eksperimentalnaya Khimiya*, 1998, **34**, 265.
20 J. Parmentier, J. Patarin, J. C. Dentzer and C. Vix-Guterl, *Ceram. Int.*, 2002, **28**, 1.
21 J. B. Claridge, A. P. E. York, A. J. Brungs, C. Marquez-Alvarez, J. Sloan, S. C. Tsang and M. L. H. Green, *J. Catal.*, 1998, **180**, 85.
22 K. Sonnenburg, P. Adelhelm, M. Antonietti, B. Smarsly, R. Nöske and P. Strauch, *Phys. Chem. Chem. Phys.*, 2006, **8**, 3561.
23 I. K. Sung, S. B. Yoon, J. S. Yu and D. P. Kim, *Chem. Commun.*, 2002, 1480.
24 J. M. Qian, H. P. Wang, Z. H. Jin and G. J. Qiao, *Mater. Sci. Eng., A*, 2003, **358**, 304.
25 K. H. Park, I. K. Sung and D. P. Kim, *J. Mater. Chem.*, 2004, **14**, 3436.

26 P. Krawiec, C. Weidenthaler and S. Kaskel, *Chem. Mater.*, 2004, **16**, 2869.
27 A. H. Lu, W. Schmidt, W. Kiefer and F. Schuth, *J. Mater. Sci.*, 2005, **40**, 5091.
28 Y. F. Shi, Y. Meng, D. H. Chen, S. J. Cheng, P. Chen, T. F. Yang, Y. Wan and Y. D. Zhao, *Adv. Funct. Mater.*, 2006, **16**, 561.
29 Z. H. Bao, M. R. Weatherspoon, S. Shian, Y. Cai, P. D. Graham, S. M. Allan, G. Ahmad, M. B. Dickerson, B. C. Church, Z. T. Kang, H. W. Abernathy, C. J. Summers, M. L. Liu and K. H. Sandhage, *Nature*, 2007, **446**, 172.
30 N. H. Hai, I. Grigoriants and A. Gedanken, *J. Phys. Chem. C*, 2009, **113**, 10521.
31 Y. Shi, F. Zhang, Y.-S. Hu, X. Sun, Y. Zhang, H. I. Lee, L. Chen and G. D. Stucky, *J. Am. Chem. Soc.*, 2010, **132**, 5552.
32 Y. Lei, C. Fournier, J. L. Pascal and F. Favier, *Microporous Mesoporous Mater.*, 2008, **110**, 167.
33 W. Stober, A. Fink and E. Bohn, *J. Colloid Interface Sci.*, 1968, **26**, 62.
34 D. Zhao, J. Feng, Q. Huo, N. Melosh, G. H. Fredrickson, B. F. Chmelka and G. D. Stucky, *Science*, 1998, **279**, 548.
35 K. Szczodrowski, B. Prelot, S. Lantenois, J. Zajac, M. Lindheimer, D. Jones, A. Julbe and A. van der Lee, *Microporous Mesoporous Mater.*, 2008, **110**, 111.
36 R. A. Cutler and K. M. Rigtrup, *J. Am. Ceram. Soc.*, 1992, **75**, 36.
37 S. K. Ko, C. W. Won, B. S. Chun, H. W. Kim and G. C. Shim, *J. Kor. Inst. Met. Mater.*, 1994, **32**, 1442.
38 S. T. Gregg, K. S. W. Sing, *Adsorption, Surface Area and Porosity*, Academic Press, 2nd edn, 1997.
39 H. X. Zhang, P. X. Feng, V. Makarov, B. R. Weiner and G. Morell, *Mater. Res. Bull.*, 2009, **44**, 184.
40 D. Olego and M. Cardona, *Phys. Rev. B*, 1982, **25**(6), 3889.
41 W. H. C. Rueggerberg, *J. Am. Chem. Soc.*, 1943, **65**(4), 602.
42 R. Ryoo, S. H. Joo, M. Kruk and M. Jaroniec, *Adv. Mater.*, 2001, **13**, 677.
43 B. Wen, J. J. Zhao and T. J. Li, *Int. Mater. Rev.*, 2007, **52**, 131.

